Low-Temperature Aluminum Reduction of Graphene Oxide, Electrical Properties, Surface Wettability, and Energy Storage Applications

Dongyun Wan,[†,§] Chongyin Yang,[†,§] Tianquan Lin,[†] Yufeng Tang,[†] Mi Zhou,[†] Yajuan Zhong,[†] Fuqiang Huang,[†,‡,*] and Jianhua Lin[‡,*]

[†]CAS Key Laboratory of Materials for Energy Conversion, Shanghai Institute of Ceramics, Chinese Academy of Sciences, Shanghai 200050, People's Republic of China, and [‡]State Key Laboratory of Rare Earth Materials Chemistry and Applications, College of Chemistry and Molecular Engineering, Peking University, Beijing 100871, People's Republic of China. [§]These authors contributed equally to this work.

ABSTRACT Low-temperature aluminum (Al) reduction is first introduced to reduce graphene oxide (GO) at 100–200 °C in a two-zone furnace. The melted Al metal exhibits an excellent deoxygen ability to produce well-crystallized reduced graphene oxide (RGO) papers with a low O/C ratio of 0.058 (Al-RGO), compared with 0.201 in the thermally reduced one (T-RGO). The Al-RGO papers possess outstanding mechanical flexibility and extremely high electrical conductivities (sheet resistance $R_s \sim 1.75\ \Omega$/sq), compared with 20.12 Ω/sq of T-RGO. More interestingly, very nice hydrophobic nature (90.5°) was observed, significantly superior to the reported chemically or thermally reduced papers. These enhanced properties are attributed to the low oxygen content in the RGO papers. During the aluminum reduction, highly active H atoms from H_2O reacted with melted Al promise an efficient oxygen removal. This method was also applicable to reduce graphene oxide foams, which were used in the GO/SA (stearic acid) composite as a highly thermally conductive reservoir to hold the phase change material for thermal energy storage. The Al-reduced RGO/SnS_2 composites were further used in an anode material of lithium ion batteries possessing a higher specific capacity. Overall, low-temperature Al reduction is an effective method to prepare highly conductive RGO papers and related composites for flexible energy conversion and storage device applications.

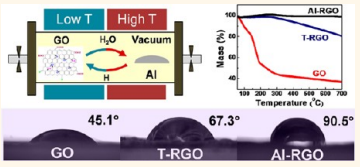

KEYWORDS: graphene oxide · Al reduction · surface wettability · thermal energy storage · lithium ion battery

Graphene, with a two-dimensional (2D) structure consisting of sp^2-bonded carbon atoms, has attracted tremendous attention from both fundamental research and promising applications in recent years due to its unique structural and physical properties.[1] Graphene holds great promise for many applications, such as nanoelectronics,[2,3] sensors,[4,5] nanocomposites,[6,7] batteries,[8] super capacitors, and hydrogen storage.[9] Graphene oxide (GO) is a promising alternative for bulk production of graphene-based materials as it can be synthesized in large quantities from inexpensive graphite powder and solubilized in a variety of solvents.[10–13] A critical challenge for technological applications of GO is that it is electrically insulating owing to the disruption of graphitic networks,[12] which can be tuned and partially recovered to produce electrically conducting material (RGO) by chemical reduction and thermal annealing.[14]

Generally, the chemical reduction of GO was carried out using a strong reductant,[15–20] including hydrazine,[15] hydroquinone,[16] and $NaBH_4$.[17] These hazardous or poisonous reagents can only partially remove the oxygen-containing groups, and the molar ratios of oxygen and carbon are 0.209–0.083 in the reported RGO products. Some metal powders (*e.g.*, Fe and Al) were reported to be added in the acidic solution to reduce GO,[21,22] whose mechanism is similar to the above-mentioned reductants. Alternatively, thermal annealing in Ar or H_2 or ultrahigh vacuum (UHV) was reported to remove oxygen effectively, and the O/C ratio is 0.297–0.117.[12,13,23,24] The electrical conductivities of the chemical or thermal reduction samples were reported to range from 1660 to 20 200 S/m.[15,23,25,26] It is noted that a low O/C ratio ensures good properties of electrical or thermal transport and high-temperature annealing benefits to lower the O/C ratio. Some RGO films on flexible substrates demand excellent electrical and mechanical properties, which have to be handled at low temperature. Therefore,

* Address correspondence to huangfq@mail.sic.ac.cn, jhlin@pku.edu.cn.

Received for review July 18, 2012 and accepted September 17, 2012.

Published online September 17, 2012
10.1021/nn303228r

it is still a great challenge to develop a low-temperature, green, and easy approach to the large-scale synthesis of RGO dispersions combining electronically superior conductivity, high mechanical flexibility, and high chemical stability.

We propose a novel environmentally friendly and efficient route to reduce graphene oxide by using elemental aluminum as the reducant in a two-zone vacuum furnace. The schematic of the equipment is shown in Figure 1. The GO sample and Al powder are initially placed in the low- and high-temperature zones, respectively. During the thermal annealing at 100–200 °C in vacuum, the oxygen-containing groups of the GO are gradually expected to disengage and achieve a chemical equilibrium. The Al powder in the high-temperature zone (800 °C) is melted. Small amount of H_2O in the chamber reacts with the melted Al to generate active H atoms, and the H atoms migrate to the low-temperature zone to reduce GO and form H_2O, CO_2, and so on. H_2O here acts like a catalyst to react with the melted Al to generate active H atoms (see the detailed discussion later). Therefore, the oxygen-containing groups in GO can be efficiently removed, and the O/C ratio is expected to be lower than that of conventional solution-based reduction and high-temperature thermal annealing.

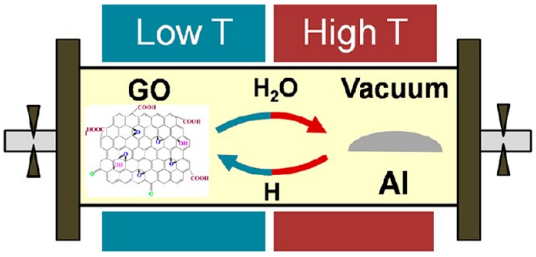

Figure 1. Schematic low-temperature reduction of graphene oxide in a two-zone furnace.

In this paper, the RGO papers were prepared by aluminum reduction. Structural and compositional investigations (Raman, XPS, TEM, *etc.*) demonstrated that the Al-RGO papers possess better crystallinity and lower O/C ratio than the reference samples of thermal RGO. The Al-RGO papers exhibit extremely high electrical conductivities ($R_s \sim 1.75$ Ω/sq), significantly superior to the reported samples by chemical or thermal reduction. The dependence of RGO surface wettability on the O/C ratio was found. The contact angle of the water droplet decreases with the O/C ratio, which is greatly improved from 67.3° (T-RGO) to 90.5° (Al-RGO). The superior Al-RGO foams were assembled into the RGO/stearic acid (RGO/SA) for thermal energy storage. The GO/SnS_2 composites were prepared as an anode material for lithium ion batteries, presenting high conductivity and good rate performance even at high current density.

RESULTS AND DISCUSSION

Typical graphene oxide powders (~10–30 μm in size) prepared by modified Hummers' method (see Methods) are the defective honeycomb papers linked with a large amount of hydroxyl and carboxyl groups, as shown in Figure 2a. Due to the hydrophilic groups (*e.g.*, carboxyl, carbonyl, hydroxyl), the graphene oxide becomes water-soluble, which is completely different from the highly hydrophobic nature of macroscopic-size free-standing and defect-free graphene or graphite.

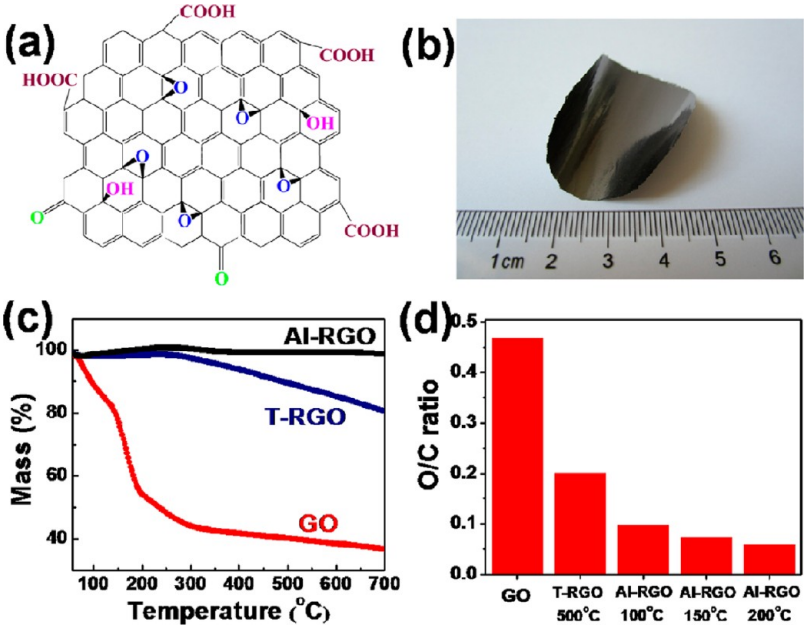

Figure 2. (a) Schematic structure of graphene oxide sheet. (b) Photograph of a typical free-standing GO paper. (c) TGA curves of the GO, T-RGO, and 200 °C Al-RGO samples. (d) Ratios of oxygen and carbon (O/C) of the samples investigated by XPS measurements.

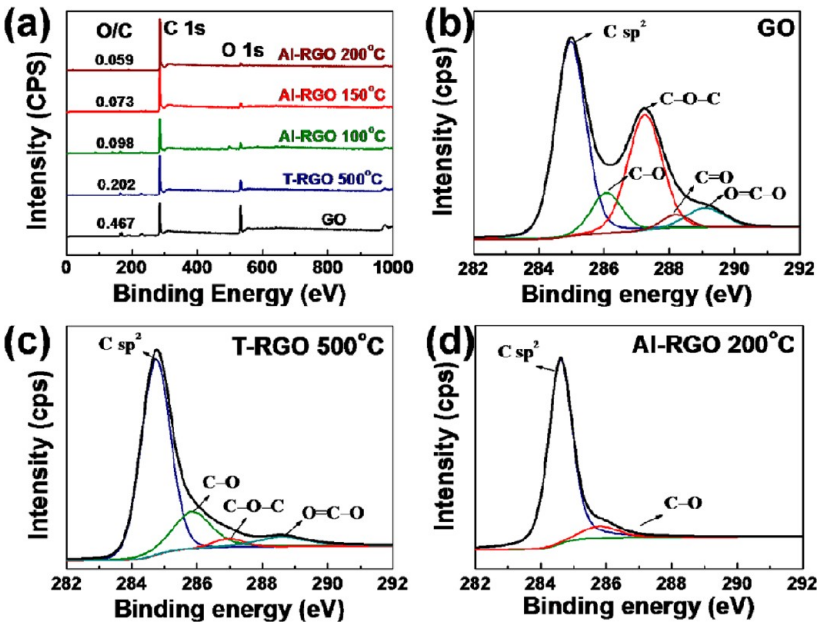

Figure 3. (a) XPS survey spectra of the as-prepared GO and RGO samples, and C 1s XPS spectra of (b) GO, (c) 500 °C T-RGO, and (d) 200 °C Al-RGO.

Herein, the graphene oxide was first reduced at 100–200 °C by melted elemental aluminum in a 0.5 Pa vacuum-sealed tube (Al-RGO), and the conventional thermal reduction was also performed to prepare a reference sample (T-RGO). The thermal stabilities of the GO and RGO were investigated by TGA, as shown in Figure 2c. The significant mass loss of GO is exhibited from about 100 to 300 °C, and the residual content is only 44.5% at 300 °C. The pyrolysis of the labile oxygen-containing functional groups was reported to yield CO, CO_2, and steam.[16] In the decomposition of 500 °C T-RGO, the residual content is 80.43% at 700 °C, suggesting the sample retains a large amount of oxygen-containing groups. Amazingly, the 200 °C Al-RGO sample has no significant mass loss in the entire process (*e.g.*, 1.2% loss at 700 °C). The TGA results are consistent with the O/C ratios in these samples (0.467 in GO, 0.201 in 500 °C T-RGO, 0.059 in 200 °C Al-RGO) from the XPS measurements, as shown in Figure 2d. Overall, the TGA analysis indicates that the nearly full reduction is achieved by aluminum reduction at 200 °C for 3 h.

The degree of GO reduction is indexed *via* the atomic ratio of oxygen and carbon (O/C) obtained from taking the ratio of C 1s peak areas in XPS spectra. The original GO signal shows two separated peaks due to the high percentage of oxygen functionalities. An initial XPS survey scan of GO reveals that the asymmetric C 1s peak can be fitted with four different peaks with binding energy at 284.6, 285.6, 286.9, and 288.6 eV, assigned to C═C, C–O, C–O–C, and O═C–O bonds, respectively (Figure 3b). The O/C ratio of the GO sample is 0.467 (Table 1), which is typical for a strongly oxidized graphite material by using the modified Hummer method. In the T-RGO sample, the

TABLE 1. Elemental Compositions (O, H) and Structural Parameters of the GO, T-RGO, and Al-RGO

sample	O/C[a]	H/C[b]	*d* (Å)[c]	$I_{D/G}$[d]
GO	0.467	0.103	9.44	1.12
T-RGO	0.201	0.028	3.68	1.06
100 °C Al-RGO	0.098	0.019	3.46	0.93
150 °C Al-RGO	0.073	0.013	3.45	0.81
200 °C Al-RGO	0.059	0.007	3.43	0.77

[a] From XPS. [b] From elemental analysis. [c] From XRD. [d] From Raman.

unpleasant bonds of C–O, C–O–C, and O═C–O are also presented in Figure 3c, and the O/C ratio is as high as 0.201. Surprisingly, the O/C ratio of 100 °C Al-RGO dropped to 0.098, which is significantly lower than the reported samples (0.297–0.117) from the conventional thermal reduction.[12,13,23,24] In the Al-reduced sample, the C═C bonds dominate by one single peak only with small tails at the higher binding energy region from C–O bonds. By increasing the reduction temperature, the ratio decreased from 0.098 (100 °C), 0.073 (150 °C), to 0.059 (200 °C), as shown in Figure S1 and Table 1. High-resolution carbon 1s peaks in the XPS spectrum indicate that the Al reduction can restore the C sp^2 network, as pointed out in the reported results.[27] More in-plane epoxide, edged carboxylate, and the others were removed in 200 °C Al-RGO, as shown in Figure 3d.

The hydrogen bonding information in the GO and Al-RGO samples is important to understand the reduction process. Therefore, the solid-state ^{13}C NMR spectra of the GO samples before and after the Al reduction were performed, as shown in Figure 4. The basic direct ^{13}C pulse magic-angle spinning (MAS) can detect all of the carbon structures, and the basic ^{1}H–^{13}C cross-polarization (CP) MAS can detect the carbon atoms

with a $^{1}H-^{13}C$ dipole–dipole interaction.[25] The ^{13}C NMR spectrum of our GO sample reveals three major signals assigned to epoxy (58.9 ppm), hydroxyl (67.3 ppm), and remaining graphitic sp^2 carbons (129.2 ppm), similar to the reported results of various graphite oxides.[17,25,28] Compared to the direct ^{13}C pulse spectrum, the $^{1}H-^{13}C$ CP preferentially enhances the tertiary alcohol C–O signal near 70 ppm (Figure 4c), consistent with a significant $^{1}H-^{13}C$ dipole–dipole interaction for the C–OH group. The corresponding NMR spectra of 200 °C Al-RGO are different, as shown in Figure 4b,d. The direct ^{13}C pulse spectrum shows an obvious upfield shift of the graphitic carbon signal by 15 ppm, which also broadens noticeably. The $^{1}H-^{13}C$ CP and direct ^{13}C pulse spectra of Al-RGO show no epoxides and alcohol (50–80 ppm region), ketones (185 ppm region), lactols (no shoulder recognizable in the 100 ppm region, much less intensity near 162 ppm), and esters (again, much less intensity near 162 ppm). Consequently, the signal of graphitic sp^2 carbon at 114.5 ppm dominates the direct ^{13}C pulse spectra of 200 °C Al-RGO (the other two peaks at 212 and 17 ppm from the MAS spinning sideband),

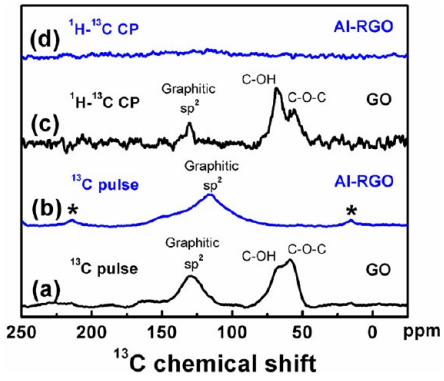

Figure 4. Solid-state ^{13}C magic-angle spinning (MAS) NMR spectra of the GO and 200 °C Al-RGO samples. (a) Direct ^{13}C pulse spectrum (with 10 kHz MAS, 11 189 scans) and (c) $^{1}H-^{13}C$ cross-polarization (CP) spectrum (with 7.5 kHz MAS, t_{cp} = 2 ms, 33 300 scans) of GO. (b) Direct ^{13}C pulse spectrum (with 10 kHz MAS, 17 104 scans) and (d) $^{1}H-^{13}C$ CP spectrum (with 7.5 kHz MAS, t_{cp} = 2 ms, 42 040 scans) of 200 °C Al-RGO. *The peaks at 212 and 17 ppm are from the MAS spinning sideband.

confirmed by the resulting 42 040-scaned CP spectrum of $^{1}H-^{13}C$ without any trace of $^{1}H-^{13}C$ dipole–dipole interaction. Therefore, the NMR investigations of direct ^{13}C pulse and $^{1}H-^{13}C$ cross-polarization spectra further verify that the Al-reduced samples contains few oxygen- or hydrogen-containing groups, which behave similar to pure graphite.[25] The elemental analyses of hydrogen and carbon were also performed to examine the NMR results, as listed in Table 1. The H/C ratio of the 200 °C Al-RGO sample is less than 0.7%, compared with 10.3% for GO and 2.8% for T-RGO. The H/C ratio of Al-RGO decreases from 1.9 to 0.7% as reduction temperature decreases from 100 to 200 °C. The high hydrogen content is associated with the high oxygen content in the sample.

Raman spectra provide additional structural information of our samples, as shown in Figure 5b. The Raman spectrum of graphene is characterized by two main features, the G mode arising from the first-order scattering of the E_{2g} phonon of C sp^2 atoms (usually observed at ~1575 cm^{-1}) and the D mode arising from a breathing mode of κ-point photons of A_{1g} symmetry (~1350 cm^{-1}).[29,30] As the Raman spectrum of GO is shown in Figure 5b, the G band broadens and shifts to 1584 cm^{-1}. Additionally, the D band at 1360 cm^{-1} is quite prominent, indicating the reduction in size of the in-plane sp^2 domains, possibly due to structural imperfections created by oxygen functional groups in the carbon basal plane.[31] After the 500 °C thermal reduction, no obvious shifts for the D band or the G band were observed. The ratio of the intensities of the D and G bands (I_D/I_G) is usually used to index the extent of modification or defects in a carbon sample.[32] The I_D/I_G ratio of thermal RGO is only 1.06, similar to GO (1.12). It may be due to unrepaired defects, dangling bonds, vacancies, or distortions of the sp^2 domains generated from the high-temperature removal of oxygen and detachment of CO groups. The I_D/I_G ratio of the 100 °C Al-RGO paper is 0.93, but it sharply decreases to 0.77 for 200 °C Al-RGO. Such a low ratio implies that the 200 °C aluminum reduction greatly restored the sp^2 network.[13]

The typical XRD patterns of the GO, Al-RGO, and thermal RGO samples are shown in Figure 5a. The XRD pattern of GO exhibits a weak (001) diffraction peak

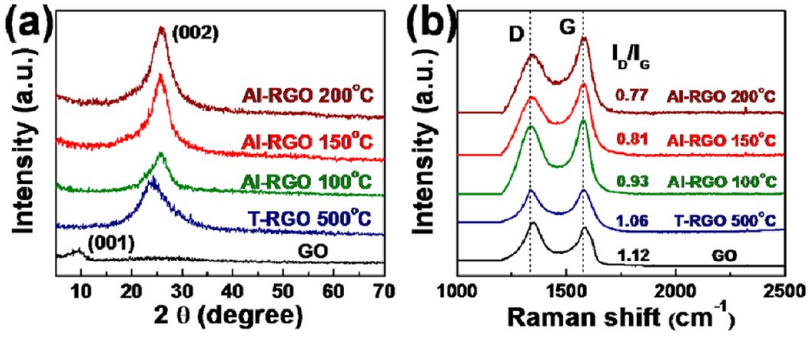

Figure 5. (a) X-ray diffraction patterns and (b) Raman spectra of the as-prepared GO and RGO samples.

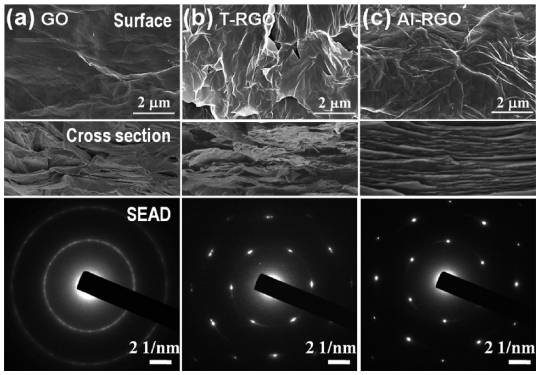

Figure 6. Surface and cross-sectional SEM images and SAED patterns of TEM images of (a) GO, (b) 500 °C T-RGO, and (c) 200 °C Al-RGO.

($2\theta \sim 9.36°$) corresponding to a large interlayer distance (~9.44 Å) (Table 1). It is due to the formation of hydroxyl, epoxy, and carboxyl groups. The T-RGO sample also has a broad (002) diffraction peak ($2\theta \sim 24.14°$), corresponding to a *d* spacing of 3.68 Å. The 100 °C Al-RGO paper possesses a broad (002) diffraction peak ($2\theta \sim 25.72°$) with the interlayer distance of 3.46 Å. The diffraction peaks of Al-RGO become sharper with the processing temperature. The interlayer distance decreases to 3.43 Å for 200 °C Al-RGO, only slightly larger than that of graphite (3.42 Å, JCPDS No. 75-1621). It demonstrates that the 200 °C Al-RGO paper is nearly fully reduced, without extra vertically erected oxygen-containing functional groups. It is evident that the Al-RGO can keep a more perfect C sp^2 structure with fewer defects.

The morphological and structural properties of the graphene materials were investigated using SEM and TEM techniques, as shown in Figure 6. The GO paper has a rough surface and entangled cross section shown in the SEM images (Figure 6a), which are generated during vacuum filtration from the GO suspension. The selected area electron diffraction pattern (SAED) is the powder rings from graphene, indicating the nature of polycrystals and imperfections. The T-RGO paper has wrinkles and folding characteristics with obvious cracks and holes (Figure 6b). The packing disorder is partially due to a large amount of the as-generated gases and thermal stress being released from the paper during high-temperature reduction. The crystallinity of T-RGO was improved as shown from its electron diffraction, but the defective and polycrystalline feature was still observed. The surface of 200 °C Al-RGO displays a corrugated morphology with many folded wrinkles, but its cross section is much better assembled and more closely packed than the GO or T-RGO paper, as shown in Figure 6c. Strong diffraction spots with sixfold rotational symmetry in the SAED pattern reveal the nearly single-crystal nature of Al-RGO, compared to the other two samples (GO, T-RGO). The outstanding structural features (see also the TEM images in Figure S2) demonstrate that the aluminum reduction is an efficient method, and the low-temperature process ensures that the original packing pattern remains, which is important to fabrication of flexible devices.

Mechanism of Aluminum Reduction. The graphene oxide sheets contain a large amount of carboxyl (O═C−OH), carbonyl (C═O), and hydroxyl (−OH) groups. The reduction of GO is a process to remove these hydrophilic groups. Traditional thermal reduction adopts the self-reduction of carbon with an oxygen-containing group at high temperature (*e.g.*, 500 °C) to form the gases (CO, H_2O, H_2, *etc.*). The well-assembled GO paper was messed up during the thermal treatment due to large amount of newly formed gases, which can explain why the T-RGO paper is much more loosely stacked.

As demonstrated by the solution reduction of GO, the H atom is an efficient reducing agent to reduce GO. Normally, the dissociation of molecular H_2 occurs at very high temperature (*i.e.*, 1100 °C) to obtain the activated atomic H.[33] The mechanism of aluminum reduction is attributed to a small amount of H_2O in the chamber rapidly reacting with the melted Al to generate active H atoms at low temperature under 0.5 Pa, and the H atoms migrate to the low-temperature zone to efficiently reduce GO to form H_2O, as shown in Figure 7a,c. Here, the H_2O molecules act like a catalyst to assist the low-temperature reduction, and the related chemical reactions are expressed in Figure 7c.

Reactions 2−4 can be initialized at 100 °C, and the reaction is apparently faster at a higher temperature. The final Al-RGO papers remain in a tight stacking form and in a better ordering after removing the erected hydrophilic groups on GO sheets. Therefore, the oxygen-containing groups are able to be removed from GO and form RGO, and the O/C ratio is expected to be lower than conventional solution-based reduction and high-temperature thermal annealing. As expected, the oxygen removal of the 200 °C Al-RGO sample (O/C ratio: 0.059) is larger than that of the 100 °C Al-RGO (O/C ratio: 0.098), much more efficient than the 500 °C thermal reduction (O/C ratio: 0.201).

In order to demonstrate the proposed reduction mechanism, the H_2 gas was pumped in at the same pressure at 100−200 °C, but the GO paper was not observed to be reduced. Furthermore, the plasma hydrogen was performed to reduce the GO paper, and the obtained result is similar to the aluminum reduction (Figure S3). It indicates that the aluminum reduction is a method based on highly active H atoms to prepare high-quality graphene from graphene oxide.

The aluminum reduction process combines the merit of the low/high-temperature compartments, where the reductant (aluminum) is melted in the high-temperature compartment and the reduction *via* a reacting gas (atomic H) is carried out in the low-temperature compartment. From an engineering viewpoint, this

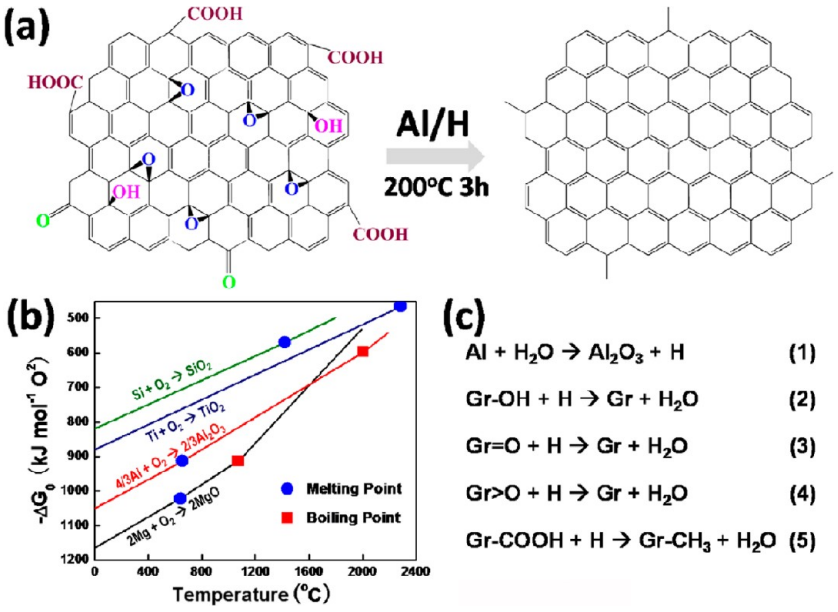

Figure 7. (a) Scheme procedure of the Al reduction of GO. (b) Partial Ellingham diagram. (c) Chemical reactions for the Al reduction of GO.

configuration allows separate control. Thermodynamically, the reaction driving force is provided by aluminum oxidation and carbon reduction, as in the Ellingham diagram[34] shown in Figure 7b. Since the free energy of reactions involving gases decreases with temperature, the driving force is larger if the reaction is carried out at a lower temperature. However, to speed up the kinetics, it is advantageous to use molten aluminum (>660 °C). Meanwhile, the actual reduction can be carried out at a much lower temperature through an intermediary—the lower limit for the reaction temperature being the temperature to initiate reaction on the graphene oxide surface. This aluminum reduction is the thermodynamic and kinetic basis of the two-compartment method.

Elemental aluminum is the optimal reductant, which can also be explained from the Ellingham diagram. Although magnesium melts at about the same temperature, its molar metal oxidation free energy is smaller than that of aluminum. Titanium and silicon have slightly larger molar metal oxidation free energies, but their melting point is much higher. Therefore, the current process may be the best one from a thermodynamic/kinetic standpoint, which may also promise the excellent transport properties of the Al-RGO samples for the applications.

Electrical Properties. As discussed above, the aluminum reduction can remove more oxygen-containing groups with a lower O/C ratio and remain a perfect C sp^2 structure with fewer defects than the thermal reduction. Furthermore, the Al-reduced graphene oxide paper is more orderly packed. As expected, the 200 °C Al-RGO paper should possess the best electric transport properties among all of the investigated samples due to the consideration of the O/C ratio. The plot of sheet resistance and mobility depending on the O/C ratio is shown in Figure 8a. By increasing the O/C ratio, the sheet resistance of the paper increases but the mobility decreases. The overall electrical conductivity of the graphene paper increases when the oxygen-containing functional groups are reduced.

Electrical properties of GO, T-RGO, and Al-RGO papers are listed in Table 2. The electrical sheet resistance (R_s) of the Al-RGO decreases with a reduction in temperature, and the conductivity increases accordingly. The 200 °C Al-RGO paper shows the electrical conductivity (σ) up to 38 100 S/m (sheet resistance (R_s) = 1.75 Ω/sq), superior to the insulating GO paper and the T-RGO paper (σ = 3310 S/cm, R_s = 20.12 Ω/sq). The reported RGO papers typically possess electrical conductivities ranging from 1660 to 20 200 S/m.[15,23,25,26] Note that even the 100 °C RGO paper with $\sigma \sim$ 4870 S/cm and $R_s \sim$ 13 Ω/sq is adequately used in current commercial energy conversion and storage devices. The mobility (μ in Table 2) of the Al-RGO paper increases with the reduction temperature, reaching 154 $cm^2\ V^{-1}\ s^{-1}$ for 200 °C Al-RGO. Even the mobility of 100 °C Al-RGO (38.9 $cm^2\ V^{-1}\ s^{-1}$) is far superior to the 500 °C T-RGO (13.1 $cm^2\ V^{-1}\ s^{-1}$). These results are all supportive of the earlier claim of fewer defects in the Al-reduced samples.

Mechanical Properties. The well-packed microstructure of the Al-RGO paper determined from SEM and TEM investigations promises its excellent mechanical flexibility. In order to evaluate the mechanical stability performance, the resistance change of the 200 °C Al-RGO papers under bend cycles using a radius of curvature of about 5 mm is shown in Figure 8b. The resistance values only increase <6% after 500-time bending distortion of R = 5 mm. The Al-RGO papers were bent down to 5−12.5 mm radius with trivial

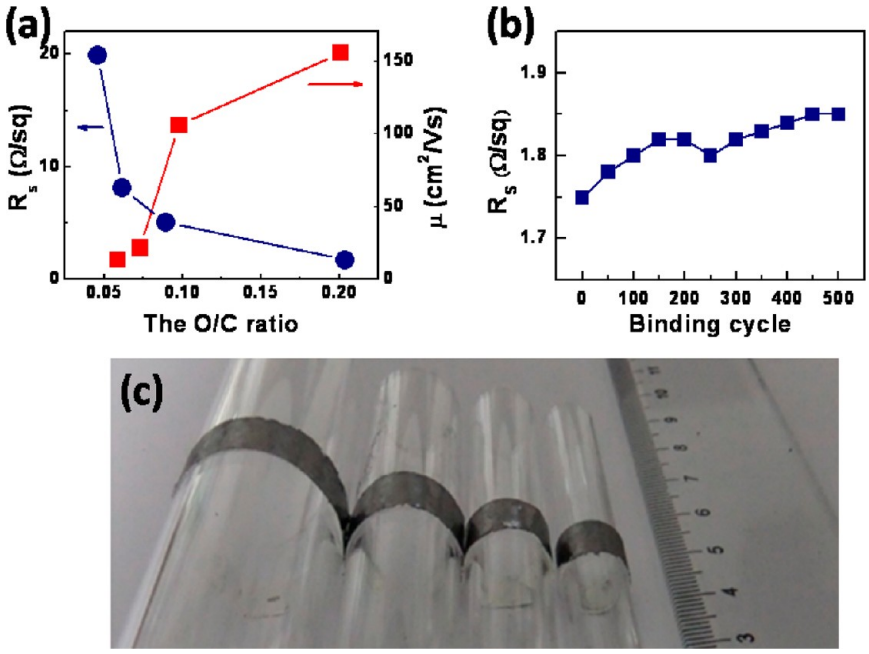

Figure 8. (a) Sheet resistance and carrier mobility for four reduced samples with different ratios of oxygen and carbon (O/C). (b) Sheet resistance deviations of the 200 °C Al-RGO papers in the bending tests at a constant radius of curvature of 5 mm. (c) Photograph of the Al-RGO papers to reveal their flexibility.

TABLE 2. Surface Wettability of Water Droplets and Electrical Properties of the GO, T-RGO, and Al-RGO Papers[a]

sample	R_s (Ω/sq)	σ (S/m)	μ (cm²/Vs)	θ_c (°)	γ (mJ/m²)
GO				45.1	54.8
T-RGO	20.12	3310	13.1	67.3	39.19
100 °C Al-RGO	13.69	4870	38.9	77.2	32.2
150 °C Al-RGO	2.77	24070	62.9	85.3	26.7
200 °C Al-RGO	1.75	38100	154	90.5	23.4
chemical RGO				44—127[35—38]	
chemical RGO		45—2300[15,25,26]			
T-RGO				82.4[39,b]	
T-RGO		5230,[23] 20200[33,c]			

[a] θ_c, contact angle; γ, specific surface energy; R_s, sheet resistance; σ, electrical conductivity; μ, carrier mobility. [b] The T-RGO sheet was covalently assembled on silicon wafers for the water contact angle measurement. [c] The T-RGO sample was annealed at 1100 °C in Ar/H_2 atmosphere.

measurable change in electrical conductivity (Figure 8c). The outstanding mechanical flexibility is likely due to the ordered packing of graphene sheets (the cross section shown in Figure 6c). The flexibility and the self-standing property of the papers provide them with potential applications in flexible electronics, energy storage, and photovoltaic devices, *etc.*

Wettability of Water Droplets. The graphene consists of a two-dimensional honeycomb carbon lattice. The stable electronic structure results in a rather low surface energy. The attraction from the nonpolar lattice to water molecules is weaker than the binding energy among water molecules. Therefore, the free-standing perfect graphene film is highly hydrophobic. Surface energy engineering, including hydrophilic group addition, carbon lattice damage (oxygen-etching, *etc.*),

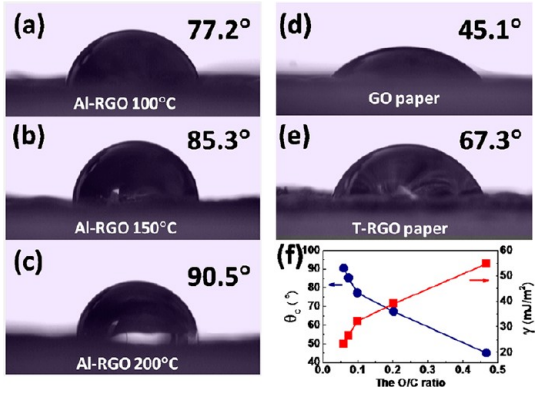

Figure 9. Photographs of water droplet on the paper of (a) 100 °C Al-RGO, (b) 150 °C Al-RGO, (c) 200 °C Al-RGO, (d) GO, and (e) 500 °C T-RGO. (f) Contact angles and surface energies of five samples with different ratios of oxygen and carbon (O/C).

substrate effect (Cu, Au, *etc.*), microstructure engineering, *etc.*, can shift the contact angle of the water droplet from 44 to 127° (nanostructured graphene composite paper).[23,35—39] The 2 in. graphene oxide sheets (Φ 5.0 cm) with thicknesses of 15 μm were used in the preparation of our graphene oxide papers. The smooth surface of our graphene papers well-assembled by graphene sheets at the size of ~10—30 μm is attributed to their wettability acting like the macroscopic-size free-standing graphene or graphite.

Static contact angles of water droplets were measured by placing a droplet of deionized water on the surface of the GO and Al-RGO papers, as shown in Figure 9. Overall, the surface energy increases but the contact angle (θ_c) decreases with increasing the O/C

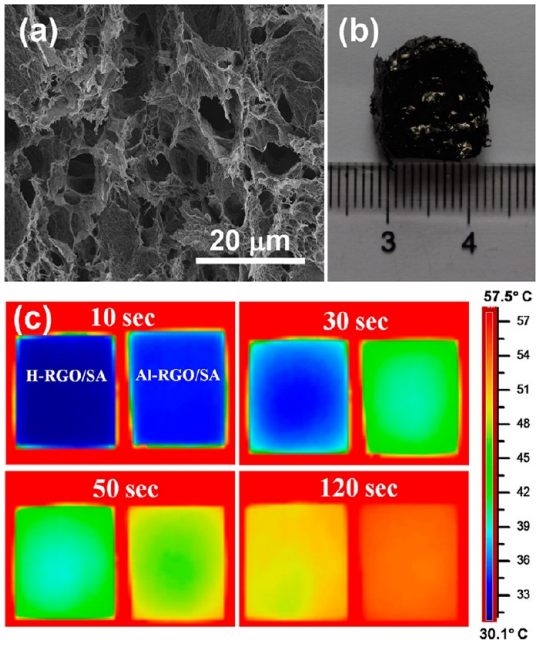

Figure 10. (a) SEM image and (b) photograph of the porous RGO foam prepared by the one-step hydrothermal method. (c) Thermal transport evolution of H-RGO/SA and Al-RGO/SA composites. The thermal images visually illustrate the excellent thermal characteristics of the Al-RGO/SA.

ratio (Figure 9f). The estimated contact angle of water on the solid surface and the calculated surface energy are listed in Table 2. The GO paper was observed to be completely wetting; that is, the water droplet brought into contact with the solid spontaneously formed a film with a water contact angle of ~45.1° (Figure 9d) with a surface energy of 54.8 mJ/m^2. The GO paper here displays high hydrophilicity. The contact angle of T-RGO increases (67.3°), and the surface energy decreases (39.2 mJ/m^2). The surface energy of Al-RGO decreases greatly from 32.2 mJ/m^2 (100 °C Al-RGO) to 23.4 mJ/m^2 (200 °C Al-RGO). The contact angle of the Al-RGO paper increases with increasing Al-reduced temperature (Figure 9a–c). The contact angle of 200 °C Al-RGO reaches 90.5°, similar to the epitaxial graphene on SiC (92.5°) and freshly cleaved highly ordered pyrolytic graphite (HOPG, 91°).[40] It again demonstrates that the defects in 200 °C Al-RGO are rather low and the aluminum reduction is an effective method.

Thermal Energy Storage. The aluminum reduction process was also used to further treat hydrothermally reduced graphene oxide foams (H-RGO) (see Methods). The SEM image and the photograph of the H-RGO foam clearly illustrate a porous structure, as shown in Figure 10a,b. The H-RGO foam was further reduced by elemental aluminum at 200 °C (Al-RGO). The sheet resistance of the H-RGO foam is over 1800 Ω/sq, and the R_s of the Al-RGO foam decreases to 24 Ω/sq. As demonstrated above, the Al-reduced graphene sheets contain very few defects to promise high electrical and thermal conductivities. The highly electrically conductive Al-RGO foam is a perfect reservoir to accommodate a phase change material (*i.e.*, stearic acid (SA)) for thermal energy storage.

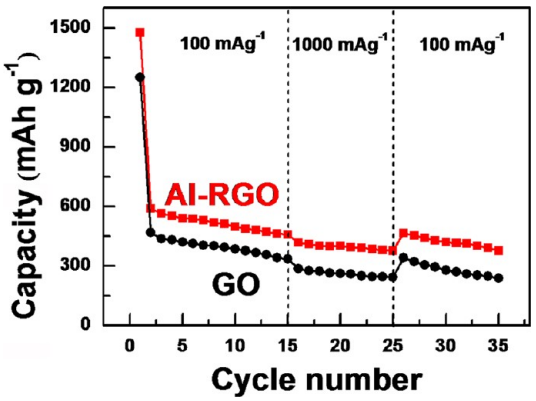

Figure 11. Rate performance of the GO/SnS_2 composite before and after being reduced *via* Al powder.

The stearic acid (SA) was infiltrated into porous graphene foams to obtain the thermal energy storage device of the RGO/SA composite. The composite foam without Al reduction treatment (H-RGO/SA) is also characterized for comparison. Temperature distribution images of H-RGO/SA and Al-RGO/SA during the heating times of 10, 30, 50, and 120 s are shown in Figure 10c. In the first 10 s period, temperature distribution is almost the same. By increasing the heating time, the Al-RGO/SA composite has a faster thermal response than H-RGO/SA. The image color of Al-RGO/SA changed quickly from blue to red, faster than H-RGO/SA. It is due to the higher thermal conduction of Al-RGO for more rapid heat transfer. The results shown in Figure 10c are all supportive of the earlier claim of fewer defects in our samples. The as-prepared Al-RGO/SA composites can potentially be applied as a thermal management material in electronics.

Conductive Additive Material in Lithium Batteries. Graphene oxide has been used as a conductive additive material in the electrode materials of lithium batteries. However, the chemically reduced graphene oxide cannot ensure its high electrical conductivity. The aluminum reduction can be performed at low temperature (≤200 °C) without affecting the active materials. SnS_2 has been considered as one of the most promising alternative anode materials to replace carbon due to its high theoretical gravimetric lithium storage capacity.[41–43] However, the large volume change of SnS_2 during the lithiation/delithiation process, which leads to the rapid deterioration and low retention of the capacity, limits its practical application.

One of the most promising strategies to tackle this obstacle is to construct hybrid materials with fascinating graphene. The composite consisting of Al-RGO and SnS_2 was synthesized at 200 °C for 3 h under 0.5 Pa, and the graphene additive is 2.19 wt %. Figure 11 shows the

rate performance of Al-RGO/SnS_2 and GO/SnS_2. Compared with GO/SnS_2, the Al-RGO/SnS_2 sample exhibits a higher rate capacity. At the current density of 100 mA g^{-1}, Al-RGO/SnS_2 has a capacity of 540 mAh g^{-1} after five cycles, which is much higher than 420 mAh g^{-1} of GO/SnS_2. At a high current density of 1000 mA g^{-1}, the capacity of Al-RGO/SnS_2 reaches 420 mAhg^{-1}, and the value of GO/SnS_2 is only 242 mAh g^{-1}. From 540 mAhg^{-1} at 100 mA g^{-1} to 420 mAhg^{-1} at 1000 mA g^{-1}, the capacity retention of Al-RGO/SnS_2 remains as high as 77.8%. The excellent rate capability should be ascribed to the advantageous combination of Al-RGO and SnS_2, wherein the graphene acts as a good buffering matrix and provides a highly conductive network.

CONCLUSIONS

We have demonstrated a green and facile reduction approach to prepare the RGO papers by using the melted elemental Al as the reductant in a two-zone furnace. Highly conductive and flexible RGO papers were fabricated by the newly developed low-temperature reduction (100−200 °C). The Al-RGO papers have a well-assembled structure with nice hydrophobic nature due to an excellent ability to remove oxygen functionalities during the process. The mechanism of aluminum reduction is attributed to the active hydrogen atoms releasing the O-containing groups from graphene. The O/C ratio is correlated with many physical properties (the graphene packing order, electrical conductivity, wettability (surface energy, contact angle), *etc.*). The Al-RGO papers possess extremely high electrical conductivities (with electrical conductivity up to 38 100 S/m), significantly superior to the reported chemically or thermally reduced samples (~1660−20 200 S/m). Such reduction approach was also carried out to reduce the graphene foam used in the RGO/stearic acid (RGO/SA) composite for thermal energy storage and in the RGO/SnS_2 anode electrode for lithium batteries. The higher conductivity of the nearly defect-free Al-RGO allows better heat storage and higher specific capacity throughout the composites. This aluminum reduction approach offers a potential for cost-effective, environmentally friendly, and large-scale production of RGO paper and composites.

METHODS

GO Colloidal Dispersion Preparation. Graphene oxide preparation started with flake graphite (100 mesh) using a modified Hummers' method.[44,45] In a typical process, 3.0 g of graphite, 1.5 g of $NaNO_3$, and 69 mL of H_2SO_4 were stirred together in an ice bath until homogenized. After 9 g of $KMnO_4$ was slowly added to the solution while stirring, the solution was transferred to a 40 °C water bath and stirred for about 6 h to form a black thick paste. Then, 300 mL of water was added and stirred for 1 h, and then 5 mL of H_2O_2 (30 wt % aqueous solution) was added and stirred for 2 h. The bright yellow colloid was obtained. Inorganic anions and other impurities were removed through six washing cycles that included centrifugation, discarding supernatant liquid, and resuspending the solid in an aqueous mixture using stirring and ultrasonication. After drying, the loose and brown GO powder was obtained.

GO Paper Preparation. GO colloidal dispersion was assembled into a paper-like film under a directional flow. Vacuum filtration of colloidal dispersions of GO through a cellulose acetate membrane (0.22 μm pore size) filter yielded, after drying, 2 in. free-standing graphene oxide paper (Φ 5.0 cm) with thicknesses ranging from 10 to 50 μm (Figure 2b).

GO Foam Preparation. GO foam was prepared by a one-step hydrothermal method according to the reported method.[46] The 20 mL homogeneous GO aqueous dispersion (4 mg mL^{-1}) was sealed in a 50 mL Teflon-lined autoclave and maintained at 180 °C for 12 h, and the obtained GO foam was washed with distilled water and then freeze-dried.

Aluminum Reduction. The above GO samples were treated with the double temperature area reduction method using aluminum powder as the conductive agent. In this process, GO samples and aluminum were placed separately in a double temperature area tube furnace and then vacuated to a base pressure lower than 0.5 Pa. After that, aluminum was heated to 800 °C, and GO samples were heated to 100, 150, and 200 °C for 3 h for comparison. This process is a noncontact oxidation−reduction reaction method, which is totally different from the reported oxidation−reduction reaction with the reducing agent directly contacting the oxidant. For comparison, the sample by the traditional thermal reducing method was also prepared by heating the starting GO sample to 500 °C under a weak reducing atmosphere with a mixture gas of 300 sccm Ar and 15 sccm H_2 for 3 h.

Characterization and Measurement. The morphologies and structures of GO and their reduced samples were investigated with scanning electron microscope (SEM, JEOL JSM-6510 and Hitachi S-4800), X-ray diffraction (XRD, Bruker D8 Avance), high-resolution transmission electron microscopy (HRTEM, JEOL JEM 2100F), and selected area electron diffraction (SAED). Raman spectra of samples were obtained with Raman spectroscopy having a laser excitation energy of 532 nm. The electrical properties of the samples were measured by the Van der Pauw method with an Accent HL5500. Thermogravimetric analysis (TGA) was conducted on a TA Instruments Q50 by heating from room temperature to 700 at 5 °C/min in a nitrogen atmosphere. Solid-state ^{13}C magic-angle spinning (MAS) NMR spectra were acquired on a Bruker Ascend-400 spectrometer (100.6 MHz ^{13}C, 400.3 MHz ^{1}H) using standard Bruker pulse programs, as well as a modified pulse program in order to incorporate dipolar dephasing into the direct ^{13}C pulse experiment. Elemental analysis was performed using an elementar vario MICRO cube. Water contact angles of the samples were measured with a Data-Physics OCA 20 (Germany) at room temperature. A 2 μL water droplet was used in the measurement. Temperature distribution images of the samples were recorded by a thermal imager (sc305, flir USA).

The charge and discharge capacities were measured with coin cells in which a lithium metal foil was used as the counter electrode. The electrolyte employed was a 1 M solution of $LiPF_6$ in ethylene carbonate and dimethyl carbonate (EC + DMC) (1:1 in volume). The active material powder (80 wt %), acetylene black (10 wt %), and polyvinylidene fluoride (PVDF) binder (10 wt %) were homogeneously mixed in NMP solvent with magnetic stirring. After stirring for 3.5 h, the slurry was coated uniformly on a copper foil. Finally, the electrode was dried under vacuum at 110 °C for 10 h. Cell assembly was carried out in an argon-filled glovebox (M. Braun Co., Germany, [O_2] < 1 ppm, [H_2O] < 1 ppm). The coin cells were cycled under different current densities between cutoff voltages of 1.5 and 0.01 V on a CT2001A cell test instrument (LAND Electronic Co.) at room temperature.

Conflict of Interest: The authors declare no competing financial interest.

Acknowledgment. Financial support from National 973 and 863 Program of China Grant Nos. 2009CB939903 and 2011AA050505, NSF of China Grant Nos. 11274328, 51125006, 91122034, 51121064, 51102263, 21101164, and 61076062, NSF of Shanghai Grant No. 11ZR1441900, and STC of Shanghai Grant No. 10JC1415800 is acknowledged.

Supporting Information Available: C 1s XPS spectra of GO papers reduced *via* Al powder under different temperatures; C 1s XPS spectra of GO paper reduced by the plasma hydrogen; TEM images of GO and RGO papers. This material is available free of charge *via* the Internet at http://pubs.acs.org.

REFERENCES AND NOTES

1. Katsnelson, M. Graphene: Carbon in Two Dimensions. *Mater. Today* **2007**, *10*, 20–27.
2. Avouris, P.; Chen, Z.; Perebeinos, V. Carbon Based Electronics. *Nat. Nanotechnol.* **2007**, *2*, 605–615.
3. Son, Y.; Cohen, M.; Louie, S. Half-Metallic Graphene Nanoribbons. *Nature* **2006**, *444*, 347–349.
4. Schedin, F.; Geim, A. K.; Morozov, K. S.; Hill, E.; Blake, P.; Katsnelson, M.; Novoselov, K. Detection of Individual Gas Molecules Adsorbed on Graphene. *Nat. Mater.* **2007**, *6*, 652–655.
5. Sakhaee-Pour, A.; Ahmadian, M.; Vafai, A. Potential Application of Single-Layered Graphene Sheet as Strain Sensor. *Solid State Commun.* **2008**, *147*, 336–340.
6. Stankovich, S.; Dikin, D. A.; Dommett, G. H. B.; Kohlhaas, K. M.; Zimney, E. J.; Stach, E. A.; Piner, R. D.; Nguyen, S. T.; Ruoff, R. S. Graphene-Based Composite Materials. *Nature* **2006**, *442*, 282–286.
7. Watcharotone, S.; Dikin, D.; Stankovich, S.; Piner, R.; Jung, I.; Dommett, G.; Evmenenko, G.; Wu, S.; Chen, S.; Liu, C. Graphene−Silica Composite Thin Films as Transparent Conductors. *Nano Lett.* **2007**, *7*, 1888–1892.
8. Takamura, T.; Endo, K.; Fu, L.; Wu, Y.; Lee, K.; Matsumoto, T. Identification of Nano-Sized Holes by TEM in the Graphene Layer of Graphite and the High Rate Discharge Capability of Li-Ion Battery Anodes. *Electrochim. Acta* **2007**, *53*, 1055–1061.
9. Novoselov, K. S.; Jiang, D.; Schedin, F.; Booth, T. J.; Khotkevich, V. V.; Morozov, S. V.; Geim, A. K. Two-Dimensional Atomic Crystals. *Proc. Natl. Acad. Sci. U.S.A.* **2005**, *102*, 10451–10453.
10. Loh, K. P.; Bao, Q. L.; Ang, P. K.; Yang, J. X. The Chemistry of Graphene. *J. Mater. Chem.* **2010**, *20*, 2277–2289.
11. Steurer, P.; Wissert, R.; Thomann, R.; Mulhaupt, R. Functionalized Graphenes and Thermoplastic Nanocomposites Based upon Expanded Graphite Oxide. *Macromol. Rapid Commun.* **2009**, *30*, 316–327.
12. Schniepp, H. C.; Li, J. L.; McAllister, M. J.; Sai, H.; Herrera-Alonso, M.; Adamson, D. H. Functionalized Single Graphene Sheets Derived from Splitting Graphite Oxide. *J. Phys. Chem. B* **2006**, *110*, 8535–8539.
13. Zhang, H. B.; Wang, J. W.; Yan, Q.; Zheng, W. G.; Chen, C.; Yu, Z. Z. Vacuum-Assisted Synthesis of Graphene from Thermal Exfoliation and Reduction of Graphite Oxide. *J. Mater. Chem.* **2011**, *21*, 5392–5397.
14. Park, S.; Ruoff, R. S. Chemical Methods for the Production of Graphenes. *Nat. Nanotechnol.* **2009**, *4*, 217–224.
15. Stankovich, S.; Dikin, D. A.; Piner, R. D.; Kohlhaas, K. A.; Kleinhammes, A.; Jia, Y.; Wu, Y.; Nguyen, S. T.; Ruoff, R. S. Synthesis of Graphene-Based Nanopapers *via* Chemical Reduction of Exfoliated Graphite Oxide. *Carbon* **2007**, *45*, 1558–1565.
16. Wang, G.; Yang, J.; Park, J.; Gou, X.; Wang, B.; Liu, H. Facile Synthesis and Characterization of Graphene Nanopapers. *J. Phys. Chem. C* **2008**, *112*, 8192–8195.
17. Si, Y.; Samulski, E. T. Synthesis of Water Soluble Graphene. *Nano Lett.* **2008**, *8*, 1679–1682.
18. Wu, Z. S.; Ren, W. C.; Gao, L. B.; Liu, B. L.; Jiang, C. B.; Cheng, H. M. Synthesis of High-Quality Graphene with a Predetermined Number of Layers. *Carbon* **2009**, *47*, 493–499.
19. Becerril, H. A.; Mao, J.; Liu, Z.; Stoltenberg, R. M.; Bao, Z.; Chen, Y. Evaluation of Solution-Processed Reduced Graphene Oxide Films as Transparent Conductors. *ACS Nano* **2008**, *2*, 463–470.
20. Dubin, S.; Gilje, S.; Wang, K.; Tung, V. C.; Cha, K.; Hall, A. S. A One-Step, Solvothermal Reduction Method for Producing Reduced Graphene Oxide Dispersions in Organic Solvents. *ACS Nano* **2010**, *4*, 3845–3852.
21. Fan, Z. J.; Wang, K.; Yan, J.; Wei, T.; Zhi, L. J.; Feng, J.; Ren, Y. M.; Song, L. P.; Wei, F. Facile Synthesis of Grapheme Nanopapers *via* Fe Reduction of Exfoliated Graphite Oxide. *ACS Nano* **2011**, *5*, 191–198.
22. Fan, Z. J.; Wang, K.; Wei, T.; Yan, J.; Song, L. P.; Shao, B. An Environmentally Friendly and Efficient Route for the Reduction of Grapheme Oxide by Aluminum Powder. *Carbon* **2010**, *48*, 1670–1692.
23. Zhu, Y. W.; Stoller, M. D.; Cai, W. W.; Velamakanni, A.; Piner, R. D.; Chen, D. Exfoliation of Graphite Oxide in Propylene Carbonate and Thermal Reduction of the Resulting Graphene Oxide Platelets. *ACS Nano* **2010**, *4*, 1227–1233.
24. Compton, O. C.; Jain, B.; Dikin, D. A.; Abouimrane, A.; Amine, K.; Nguyen, S. T. Chemically Active Reduced Graphene Oxide with Tunable C/O Ratios. *ACS Nano* **2011**, *5*, 4380–4391.
25. Gao, W.; Alemany, L. B.; Ci, L. J.; Ajayan, P. M. New Insights into the Structure and Reduction of Graphite Oxide. *Nat. Chem.* **2009**, *1*, 403–408.
26. Shin, H. J.; Kim, K. K.; Benayad, A.; Yoon, S. M.; Park, H. K.; Jung, I. S.; Jin, M. H.; Jeong, H. K.; Kim, J. M.; Choi, J. Y.; *et al.* Efficient Reduction of Graphite Oxide by Sodium Borohydride and Its Effect on Electrical Conductance. *Adv. Funct. Mater.* **2009**, *19*, 1987–1992.
27. Schniepp, H. C.; Li, J. L.; McAllister, M. J.; Sai, H.; Herrera-Alonso, M.; Adamson, D. H.; Prud'homme, R. K.; Car, R.; Saville, D. A.; Aksay, I. A. Functionalized Single Graphene Papers Derived from Splitting Graphite Oxide. *J. Phys. Chem. B* **2006**, *110*, 8535–8539.
28. Stankovich, S.; *et al.* Synthesis of Graphene-Based Nanosheets *via* Chemical Reduction of Exfoliated Graphite Oxide. *Carbon* **2007**, *45*, 1558–1565.
29. Tuinstra, F.; Koenig, J. L. Raman Spectrum of Graphite. *J. Chem. Phys.* **1970**, *53*, 1126–1130.
30. Kudin, K. N.; Ozbas, B.; Schniepp, H. C.; Prud'homme, R. K.; Aksay, I. A.; Car, R. Raman Spectra of Graphite Oxide and Functionalized Graphene Papers. *Nano Lett.* **2008**, *8*, 36–41.
31. Ferrari, A. C.; Robertson, J. Interpretation of Raman Spectra of Disordered and Amorphous Carbon. *Phys. Rev. B* **2000**, *61*, 14095–14107.
32. Choucair, M.; Thordarson, P.; Stride, J. A. Gram-Scale Production of Graphene Based on Solvothermal Synthesis and Sonication. *Nat. Nanotechnol.* **2009**, *4*, 30–33.
33. Gao, W.; Alemany, L. B.; Ci, L.; Ajayan, P. M. New Insights into the Structure and Reduction of Graphite Oxide. *Nat. Chem.* **2009**, *1*, 403–408.
34. Ellingham, H. J. T. *J. Soc. Chem. Ind.* **1944**, *63*, 125–133.
35. Zhang, J.; Lei, J. P.; Pan, R.; Xue, Y. D.; Ju, H. X. Highly Sensitive Electrocatalytic Biosensing of Hypoxanthine Based on Functionalization of Graphene Sheets with Water-Soluble Conducting Graft Copolymer. *Biosens. Bioelectron.* **2010**, *26*, 371–376.
36. Tu, W. W.; Lei, J. P.; Zhang, S. Y.; Ju, H. X. Characterization, Direct Electrochemistry, and Amperometric Biosensing of Graphene by Noncovalent Functionalization with Picket-Fence Porphyrin. *Chem.—Eur. J.* **2010**, *16*, 10771–10777.
37. Khatayevich, D.; So, C. R.; Hayamizu, Y. H.; Gresswell, C.; Sarikaya, M. Controlling the Surface Chemistry of Graphite by Engineered Self-Assembled Peptides. *Langmuir* **2012**, *28*, 8589–8593.
38. Wang, S. R.; Zhang, Y.; Abidi, N.; Cabrales, L. Wettability and Surface Free Energy of Graphene Films. *Langmuir* **2009**, *25*, 11078–11081.
39. Ou, J. F.; Wang, J. Q.; Liu, S.; Mu, B.; Ren, J. F.; Wang, H. G.; Yang, S. R. Tribology Study of Reduced Graphene Oxide Sheets on Silicon Substrate Synthesized *via* Covalent Assembly. *Langmuir* **2010**, *26*, 15830–15836.

40. Shin, Y. J.; Wang, Y. Y.; Huang, H.; Kalon, G.; Wee, A. T. S.; Shen, Z. X.; Bhatia, C. S.; Yang, H. S. Surface-Energy Engineering of Graphene. *Langmuir* **2010**, *26*, 3798–3802.
41. Zai, J.; Wang, K.; Su, Y.; Qian, X.; Chen, J. High Stability and Superior Rate Capability of Three-Dimensional Hierarchical SnS_2 Microspheres as Anode Material in Lithium Ion Batteries. *J. Power Sources* **2011**, *196*, 3650–3654.
42. Zhai, C.; Du, N.; Zhang, H.; Yang, D. Large-Scale Synthesis of Ultrathin Hexagonal Tin Disulfide Nanosheets with Highly Reversible Lithium Storage. *Chem. Commun.* **2011**, *47*, 1270–1272.
43. Liu, S.; Yin, X.; Chen, L.; Li, Q.; Wang, T. Synthesis of Self-Assembled 3D Flowerlike SnS_2 Nanostructures with Enhanced Lithium Ion Storage Property. *Solid State Sci.* **2010**, *12*, 712–718.
44. Hummers, W. S.; Offeman, R. E. Preparation of Graphitic Oxide. *J. Am. Chem. Soc.* **1958**, *80*, 1339–1339.
45. Cote, L. J.; Kim, F.; Huang, J. X. Langmuir–Blodgett Assembly of Graphite Oxide Single Layers. *J. Am. Chem. Soc.* **2009**, *131*, 1043–1049.
46. Xu, Y. X.; Sheng, K. X.; Li, C.; Shi, G. Q. Self-Assembled Graphene Hydrogel *via* a One-Step Hydrothermal Process. *ACS Nano* **2010**, *4*, 4324–4330.